Correction of Excessive Precipitation over Steep and High Mountains in a GCM

Winston C. Chao

Global Modeling and Assimilation Office

NASA/Goddard Space Flight Center

Greenbelt, MD 20771

Submitted to JAS, August 20, 2011

Revised, Nov. 25, 2011, Accepted, Nov. 30, 2011

Corresponding Author Address
Dr. Winston C. Chao
Mail Code 610.1
NASA/Goddard Space Flight Center
Greenbelt, MD 20771
Winston.c.chao@nasa.gov

Abstract

Excessive precipitation over steep and high mountains (EPSM) is a well-known problem in GCMs and meso-scale models. This problem impairs simulation and data assimilation products. Among the possible causes investigated in this study, we found that the most important one, by far, is a missing upward transport of heat out of the boundary layer due to the vertical circulations forced by the daytime upslope winds, which are forced by the heated boundary layer on subgrid-scale slopes. These upslope winds are associated with large subgrid-scale topographic variation, which is found over steep and high mountains. Without such subgrid-scale heat ventilation, the resolvable-scale upslope flow in the boundary layer generated by surface sensible heat flux along the mountain slopes is excessive. Such an excessive resolvable-scale upslope flow combined with the high moisture content in the boundary layer results in excessive moisture transport toward mountaintops, which in turn gives rise to EPSM. Other possible causes of EPSM that we have investigated include 1) a poorly-designed horizontal moisture flux in the terrain-following coordinates, 2) the condition for cumulus convection being too easily satisfied at mountaintops, 3) the presence of conditional instability of the computational kind, and 4) the absence of blocked flow drag. These are all minor or inconsequential.

We have parameterized the ventilation effects of the subgrid-scale heated-slope-induced vertical circulation (SHVC) by removing heat from the boundary layer and depositing it in layers higher up when the topographic variance exceeds a critical value. Test results using NASA/Goddard's GEOS-5 GCM have shown that this largely solved the EPSM problem.

1. Introduction

It has long been known that *e*xcessive *p*recipitation over regions with *s*teep and high *m*ountains (hereafter, EPSM) in monthly or seasonal means in warm seasons is a problem in atmospheric models. These regions include the Andes (more pronounced in the Dec-Jan-Feb (DJF) season), New Guinea (in all seasons) and the Himalayas (in the Jun-Jul-Aug (JJA) season), among others. The affected regions also exhibit an excessively large amplitude in their precipitation diurnal cycle. EPSM is an obvious problem in the NASA/Goddard Space Flight Center's Earth Observing System GCM version 5 (GEOS-5). For example, the maximum DJF averaged precipitation rate over the Andes in the GEOS-5 GCM is much greater than over the Amazon and is almost double what is observed over the Amazon rainforest (as we will see later in Fig. 8). EPSM also occurs in other GCMs such as NCAR's CCSM and NOAA/GFDL's CM2 (Fig. 17 of Delworth et al. 2006). Fig. 1 of Ma et al. (2011), in a model inter-comparison of the DJF precipitation over South America, shows that most GCMs have the EPSM problem over the Andes and the few that do not have the serious problem of deficient precipitation throughout South America. The EPSM problem is more obvious in integrations with the 2°x2.5° (lat.-lon.) and 1°x1.25° grid sizes than with the 4°x5° grid size. At extremely high horizontal resolutions, such as one with a 10 km grid size, the problem diminishes considerably but is still recognizable (M.-I. Lee et al., personal communication). EPSM exists in regional models (e.g., da Rocha et al. 2009) and in multi-scale modeling framework (MMF) models (Tao et al. 2009) as well and it impairs data assimilation products (see, for example, Fig. 3 of Bosilovich et al. 2010). In the GEOS-5 GCM with a 2°x2.5° (lat.-lon.) grid size, the convective-type precipitation in the affected areas is comparable to the large-scale type precipitation. EPSM is related to large surface slope not large surface elevation, since the problem does not exist over the Tibetan Plateau but is

clearly seen over the Himalayas. It should be noted that the affected areas do have higher observed precipitation than their neighboring areas. For example, the slopes on the Himalayas have higher precipitation than in their immediate neighborhood (Fig. 1 of Oochi 1990.) But an excessive amount of precipitation in these areas in the models is a problem. This article presents our diagnosis of the problem, our solution, and its test results.

The GEOS-5 (NASA Goddard Earth Observing System, version 5) GCM is used for this study. It has the finite-volume dynamical core of Lin (2004), a combined boundary-layer and turbulence package developed from Louis (1979) for stable PBL and Lock et al. (2000) for unstable and cloud-capped PBL, the land-surface model of Koster et al. (2000), the shortwave radiation scheme of Chou and Suarez (1999), and the long-wave radiation scheme of Chou et al. (2001), the relaxed Arakawa-Schubert scheme (RAS) (Moorthi and Suarez 1992), and the prognostic cloud scheme and the rain re-evaporation scheme of Bacmeister et al. (2006). It also uses a gravity wave parameterization scheme developed from an orographic gravity wave drag scheme based on McFarlane (1987) and a scheme for non-orographic gravity waves based on Garcia and Boville (1994). The SST and surface characteristics are specified from observations. For this study, the horizontal resolution used is 2°x2.5° (lat.-lon.) There are 72 vertical levels; bottom six of them have σ values greater than 0.95.

2. Possible causes of the EPSM

For EPSM to occur, there has to be an excessive moisture supply through low-level convergence of moisture transport into the affected areas. This has several possible causes. First, if cumulus convection is somehow too easily triggered at mountaintops, the convective heating itself can induce excessive low-level moisture convergence resulting in a

feedback loop. Second, excessively strong upslope winds in the boundary layer on the resolvable scales (in the absence of too easily triggered cumulus convection) can bring excessive moisture to the high grounds. Such excessively strong upslope winds (Fig. 1) could be generated by 1) excessive daytime heating of the boundary layer along the mountain slopes, and/or 2) not enough friction to slow the winds down. The first mechanism, in turn, could be caused by excessively-high surface sensible heat flux and/or a lack of ventilation of the boundary layer heat along the mountain slopes by the *s*ubgrid-scale *h*eated-surface-induced *v*ertical *c*irculation (SHVC). SHVC is also forced by upslope winds in the boundary layer caused by heating of the sloping boundary layer due to surface sensible heat flux, but it is at the subgrid scales (Fig. 2 v. Fig. 1). SHVC is associated with large subgrid-scale topographic variation, which is found over steep and high mountains. A third possible cause for EPSM is a poorly-designed moisture transport scheme. As will be explained, the interpolation of the interface moisture between neighboring grids in the horizontal direction should recognize the variation in surface elevation. The unrealistically high low-level moisture flux can be aided by the excessive precipitation in a feedback loop, even in the cases where convection at mountaintops is not too easily triggered. We will examine each of these possible causes in detail.

We first examined the possibility of cumulus parameterization being too easily triggered at high elevations and the associated circulation then helps bring more moisture upslope to generate large-scale precipitation. In this regard, we performed some tests in which the critical cloud work function (which must be exceeded for cumulus convection to occur--see Eq. (9) of Lord et al. 1982), as used in RAS, over high terrain was raised to as high as that over the oceans. These tests did not result in any improvement. Also, since the problem does not occur over the Tibetan Plateau, where ground elevations are high, the easy triggering of cumulus convection can be discounted as a cause. In addition,

simulations with super parameterization (also called multi-scale modeling framework) could not avoid the EPSM problem (Fig. 2 of Tao et al. 2009). Thus, the cumulus parameterization can be eliminated as a contributor to EPSM.

Among the aforementioned possible causes, the unrealistically-high low-level upslope moisture flux in the problem areas caused by excessive resolvable-scale upslope winds (Fig. 1)--which blow from the low levels of the foothills toward the mountaintops during the day--turns out to be the most important. These resolvable-scale upslope winds are caused by the daytime heating of the boundary layer on the sloping sides of a mountain range through surface sensible heat flux, which creates differential heating in the horizontal direction at most levels reached by the mountains. As mentioned earlier, there are two possible reasons that this resolvable-scale upslope wind in the boundary layer could be excessive: 1) the heating of the boundary layer could be excessive and 2) there could be a lack of parameterization of the heat ventilation from the boundary layer to layers higher up. Such heat ventilation is accomplished by SHVC. For the first possibility the excessive heating of the boundary layer, leading to EPSM, could be due to excessively high ground temperature. However, since the precipitation rate in the affected areas is several fold of what is observed, even if the surface sensible heat flux is halved the problem is still sizeable. This makes the second reason--a lack of SHVC parameterization--the more reasonable cause.

Similar to the resolvable-scale upslope winds, sub-grid scale upslope winds are caused by the heating of the boundary layer by surface sensible heat flux as the result of solar radiation along the sub-grid-scale mountain slopes. Relative to the air at the same height but away from the boundary layer, the air in the boundary layer on the sub-grid-scale mountain slopes is warmer and thus rises along the slope during the daytime hours. Due to rapid heating during the daytime the boundary layer air on the sub-grid scale slopes

can be heated up very fast. The resulting SHVC, forced by such upslope winds, is upward along the slope of the sub-grid scale mountains in the boundary layer and downward away from the mountains (Fig 2). SHVC can reach heights much higher than the subgrid scale mountaintops even if it does not release latent heat (Fig. 6 of de Wekker et al. 1998). SHVC brings heat (and moisture) upward and provides a heat ventilation effect for the resolvable-scale boundary layer. Its ventilation effect is so efficient that there is little net heating in the subgrid-scale boundary layer, if the subgrid topography rises above 500m (Rampanelli et al. 2004; see their Fig. 13). This heat transport is upward regardless whether the background temperature structure is stable--as in most cases--or not. Thus, in that sense, SHVC is not the same as what modelers call "dry convection," which occurs when the vertical temperature structure on the resolvable scale is unstable.

For a GCM grid the net effect of these subgrid-scale upslope winds is to transport heat (and moisture) from the boundary layer to the layers higher up. The significance of the associated momentum transport is not expected to be great as far as EPSM is concerned for a reason that we will explain. As a consequence of the heat ventilation by SHVC, the intensity of the resolvable-scale upslope wind in the boundary layer--as discussed earlier--is substantially reduced, resulting in a much lower resolvable-scale upslope transport of moisture. Not being able to recognize this SHVC heat-ventilation effect (and to parameterize it) in the models is, by far, the most important cause of EPSM in the GCMs and in the meso-scale models.

A third possible cause of EPSM is in the formulation of the moisture transport scheme. In a GCM that uses a terrain-following vertical coordinate, if the moisture is not defined well at the interfaces between grid boxes, excessive moisture flux at these interfaces can occur. These interfaces can be either horizontal or vertical. Let's consider an extreme example of two adjacent grid boxes at the bottom level of a GCM that uses terrain-

following coordinates: box 1, which sits over the ocean, and box 2, which sits over high surface elevation, mimicking the sharp rise of the Andes (Fig. 3). Box 1, being over the ocean, has a high water-vapor mixing ratio q and, in normal circumstances, box 2, being over a high mountain and with a much lower temperature, has a very low q, even if its relative humidity is not low. If q at the interface between the boxes is defined by the moisture advection scheme as, for example, the mean of the two neighboring q's, when combined with a modest wind toward box 2 (due to the resolvable-scale upslope wind), the resulting q flux at the interface can easily transport an excessive amount of moisture to box 2 (Fig. 4). The GEOS-5 GCM uses a parabolic interpolation employing moisture at three grids, one on the downstream side and two on the upstream side. This makes things worse than a linear interpolation between two neighboring grids, when one grid sits at a high elevation and the other two sit over the ocean or flat plain on the upstream side[1]. This increased moisture flux worsens the feedback loop resulting from the lack of heat ventilation described in the preceding paragraph.

If saturated, the lower levels immediately above box 2 provide the opportunity for conditional instability of the computational kind (CICK, see p. 256 of Arakawa and Lamb (1977)), to take place. CICK can be prevented by properly designing the vertical moisture flux at the interface. However, our study of the GEOS-5 GCM indicates that CICK in the vertical direction is not a noticeable contributor to EPSM. Moreover, because of the terrain following sigma coordinate, two neighboring grids at the same sigma level in the mountainous regions can have very different heights as illustrated in Fig. 3. Thus, when both grids are saturated the horizontal moisture flux at the interface, if not properly set, can

[1] This is the situation in the foothills of mountains where air flow directed toward the mountain can bring an excessive amount of moisture into the boundary layer on the mountain slope due to the poor choice of moisture at the interface between two grids at the same level.

allow CICK to occur because the horizontal moisture flux in the sigma coordinate has a vertical component in the height coordinate in the mountainous regions.

Common to all GCMs and meso-scale models, the ground surface at the bottom of each grid column is assumed to be flat and level[2]. In reality it is neither and, due to its variation, has a larger area than a flat level surface. A larger surface area means larger soil heat and moisture capacities. Such surface characteristics have implications for all aspects of the model physics that are related to the ground surface. They can change the total energy flux received and emitted by the surface, through changes in albedo, and affect how the surface upward energy flux is partitioned among radiative, sensitive and latent heat fluxes. They can also affect the surface moisture and momentum fluxes through enlarged soil moisture capacity and enlarged surface area. Their roles in the problem of EPSM have yet to be explored. However, there are many difficulties in exploring them. One difficulty is with the incorporation of topographic variation in setting surface albedo. Another is with the assessment of sub-grid scale wind speed. In the final section of this paper we will argue that in spite of all its impacts the larger surface area should be only a minor concern in the EPSM problem.

The last possible cause we explored is not enough friction on the mountain slopes, such as a lack of blocked-flow drag over the mountain slopes (see the ECMWF/IFS documentation for a description of the blocked flow drag and its parameterization). However, incorporation of the blocked flow drag in the ECMWF model did not prevent EPSM. Hence, the lack of blocked-flow drag (or too-weak total friction in the boundary layer) is not considered as a significant contributor to the EPSM. The reason behind this finding will be discussed at the end of the next section.

[2] True for physical parameterizations. For dynamics computations the bottom surface is smooth but not necessarily level.

3. Solutions

As explained in the preceding section, SHVC transports heat upward regardless of the stability of the resolvable flow field. It also transports moisture upward. The direction of the momentum transport depends on the vertical wind profile. We assume that the sub-grid scale boundary layer upslope winds, once started, quickly reach an intensity such that, for the resolvable scales, the surface sensible heat flux entering into the boundary layer on a mountain slope is largely moved upward by SHVC to be deposited in layers well above the boundary layer, if the local sub-grid scale terrain standard deviation is greater than 300 m. This assumption is supported by the numerical simulation of upslope flow by Rampanelli et al. (2004, see their figure 13 and the associated discussions), which demonstrated the near cancellation of turbulent heating in the boundary layer by the horizontal temperature advection. In other words, we assume that the net effect of the SHVC is an almost complete removal of the heating due to turbulent heat flux convergence in the resolvable-scale boundary layer (when the sub-grid scale terrain standard deviation is greater than 300m). Such a heat ventilation effect results in a drastic reduction in the intensity of the resolvable-scale upslope boundary layer wind. Given that the boundary layer in the model[3] is only about a half kilometer thick and the sub-grid terrain often rises much higher, our assumption is not unreasonable. To parameterize the effects of SHVC we simply reduce the virtual dry static energy (Sv) tendency component that is due to turbulent heat flux (at the surface it is the surface sensible heat flux) convergence in the boundary layer (the first 500m above ground), when it is positive, by multiplying it by a factor ($1-R_S$). In other

[3] In reality, the boundary layer depth is increased by topographic variation through both thermal and mechanical mechanisms.

words, after the model has computed the tendency $(\partial S_v/\partial t)_{turb}$ in the boundary layer parameterization, it is replaced by $(1-R_{Sv})$ $(\partial S_v/\partial t)_{turb}$, where R_{Sv} is a function of the standard deviation of the sub-grid scale topography (TSD) (Fig. 5): R_{Sv} = 95%, if TSD > 400m, R_{Sv} = 0, if TSD < 300m; and it is linearly interpolated if TSD is between 300 and 400 m. The values of 300 and 400m were determined by tuning. TSD should be that of the scales smaller than the grid size. However, since the data file for TSD for scales less than 10km is already available for another purpose in the model and since this file is very similar in its pattern to the TSD for scales less than the grid size, we use it as a proxy. This dataset was computed from the TOPOG30 data from US Geological Survey (with 1km resolution). This was done by first computing the running average in both zonal and meridional directions at each 1km x 1km grid with a running average window size of 10km. The running averaged dataset also has a 1km x 1km resolution. Finally, the standard deviation of the difference between the TOPOG30 data and the running average was computed within the 2°x2.5° box to give the proxy data that is used for our purpose. When the model resolution is changed, this dataset should be recomputed. In some experiments we have used all scales less than the grid size in the definition of TSD and used the corresponding critical value and have obtained similar results.

To maintain energy conservation the virtual dry static energy taken out of the boundary layer is redistributed, with a vertical weighting profile to layers in the layer between Zbot and Zbot+5.5 km above ground, where Zbot = 1.5km if TSD=300m and 2.1 km if TSD> 700m and is linearly interpolated for 300m< TSD<700m. This vertical weighting profile is set to either unity or as increasing linearly in height from 0 at Zbot to 1 at Zbot+3.5 km and then decreasing linearly to zero at 7km. The choice of 1.5 to 2.1 km for Zbot, the lowest level of redistribution, is supported by the fact that sub-grid-scale topography as given by the GTOPO30 data from the US Geological Survey (with 1km resolution) does have

such a large variation (Fig. 6). The choice of a deep layer for the redistribution is supported by the work of de Wekker et al. (1998, see its Fig. 6), which shows that the vertical circulations thermally driven by topographic variation are very deep.

In experiments shown in this paper we have used a uniform vertical weighting profile for heat redistribution. Our tests have shown that the choice of this profile is not as critical as the choice of sufficient height for Zbot. The reason is illustrated in Fig. 7, which shows that if the heat is redistributed immediately above the boundary layer (e.g., setting Zbot to 500m, as in Fig. 7b), the resultant circulation generates a large horizontal return flow at a level as low as the boundary layer (as indicated by the horizontal arrow in Fig. 7b), not well above it as in Fig. 7c. Such a return flow occurring at low levels can bring moisture into the boundary and thus the EPSM problem remains. Accordingly, it is important to set Zbot well above the boundary layer.

To do the same for the moisture tendency as is done for the virtual dry static energy tendency would be incorrect. The reason is that SHVC can transport moisture upward even when the evaporation rate is zero. Yet, ee do not have a rigorous method for how to handle the moisture transport by SHVC. We will therefore take a non-rigorous approach by setting the fractional rate of change of moisture q due to SHVC in the layers below 500m to be proportional to that of the virtual dry static energy; i.e.:

$$(\partial q/\partial t)_{SHVC}/q = \alpha\ (\partial S_v/\partial t)_{SHVC}/S_v\ [= -\alpha R_{Sv} (\partial S_v/\partial t)_{turb}/S_v]\ ,$$

where α is a proportionality factor, R_{Sv} is the reduction factor for the virtual dry static energy rate as described in the preceding paragraph and $(\partial S_v/\partial t)_{turb}$ is the rate of change of the virtual dry static energy due to turbulence flux convergence. Also, the total reduction of moisture in the first 500 m is added back in the upper layers above, as is done for the virtual dry static energy, so that moisture conservation is kept. This is a crude approach and needs to be improved in the future. Obviously, if q were uniform in height, SHVC would

not be expected to generate any change in q and our treatment for the q tendency would be incorrect unless α is set to zero. However, since q in fact is not uniform in height, this approach can be used as an interim measure. Currently α is treated as a tuning parameter whose value is set at between 0 and 5 in a series of experiments; its optimal value is to be assessed from data assimilation experiments by varying α and seeking the α value that gives the least amount of analysis increment of moisture over the mountainous regions that have more densely populated observed data in a future study. Of course, this method of using data assimilation experiments can be employed to optimize other tuning parameters in our method, or any other tuning parameter in the model as well. Tests show that adding this moisture transport (with α varying between 0 and 5) matters little as far as solving the EPSM problem is concerned. The reason is that most of the moisture that enters the foothills of a steep and high mountain end up being precipitated during its travel upslope and α only affect how soon the moisture is precipitated out.

The same parameterization method for moisture cannot be used for momentum, since the vertical profile of momentum is very different from that of moisture; transport of momentum by SHVC does not necessarily mean a reduction of momentum in the boundary layer. Currently, nothing is done for the SHVC momentum tendency for want of theoretical guidance. Since adding or subtracting friction in the boundary layer does not have any significant impact on the EPSM problem--as will be explained at the end of this section, not doing anything about the SHVC momentum transfer is an acceptable temporary measure as far as solving the EPSM problem is concerned.

In our solution dealing with the moisture fluxes, both horizontal and vertical moisture fluxes at the interface between grid boxes are modified. For the vertical moisture flux, if two neighboring boxes in the vertical direction are saturated and if the vertical motion at the interface is upward, the moisture at the interface is set to the mixing ratio of

the upper grid box in order to prevent CICK from occurring. This solution is slightly different from that proposed by Arakawa and Lamb (1977). Our solution gives no increase of q to the upper box (if it is saturated) due to the moisture flux at the interface, and as a result, the moisture flux at the interface does not contribute to the heating of the upper box. CICK is thereby avoided. The GEOS-5 GCM uses a vertical remapping scheme to achieve vertical transport of various quantities, including moisture. Each time after the vertical remapping is done for moisture, we compute the vertical moisture flux and mass flux across an interface, and if the two neighboring grid boxes in the vertical direction are saturated, and if the vertical moisture flux is upward, we move moisture from the upper grid box to the lower one by such an amount such that the final vertical moisture flux is equal to the vertical mass flux times the moisture value of the upper grid box. In other words, when CICK is possible we use a downstream scheme for vertical moisture flux. This does somewhat more than what is required according to Arakawa and Lamb's (1977) analysis. This procedure is done from the mid-troposphere to the model bottom. Although this fix to prevent CICK contributes little to solving the EPSM problem, we decided to keep it, since CICK can occur, though rarely, in the model. It is our expectation that CICK cannot be the principal contributor to the EPSM problem, since CICK depends on moisture saturation, which is provided by the excessive resolvable scale upslope wind as a result of a lack of SHVC parameterization.

For the horizontal moisture flux, a similar way of setting the interface q between two neighboring grid boxes (without requiring them to be saturated) to that of the grid box over the higher surface elevation in the mountainous regions (i.e., a downstream scheme) would be too extreme. Because of the difficulty of revising the existing code in the dynamical core of GEOS-5, we chose to adopt a simple method of modifying the horizontal moisture flux at the interface while not changing the mass flux (effectively we change the

definition of the interface moisture). After the horizontal moisture flux at an interface is computed according to the existing code and before it is used to compute moisture convergence (which is then used to compute the moisture tendency due to horizontal convergence), if it is directed toward higher surface elevation, it is multiplied (in both zonal and meridional directions) by a factor of (1.-R) to reduce its magnitude. This factor is:

$$R = F * 0.00033 * |\Delta h| * \cos\varphi, \text{ if } \cos\varphi \geq 0;$$

$$R = 0, \text{ if } \cos\varphi < 0;$$

where F is a tuning parameter with a value between 0 (namely, no reduction) and 1 (namely, maximal reduction); $|\Delta h|$ (non-negative, in meters, reduced to 3000m if it exceeds 3000m) is the gradient of the surface height times 2 degrees in distance; and φ is the angle between the gradient vector of the surface height and the wind vector. Specifically, $\Delta h = \nabla h \cdot \Delta s$, where ∇h is the gradient of surface height and Δs is a distance vector of 2° in length in the direction of the wind vector. When the wind vector is perpendicular to the surface height gradient vector (i.e., $\varphi=\pi/2$.) no reduction is needed (i.e., R=0). Such a reduction in moisture flux does not affect moisture conservation. With few exceptions, $|\Delta h|$ is smaller than 3000m in a model with a 2°X2.5° grid size, and thus (1-R) is rarely close to zero, even when F is set to 1. It should also be noted that we have only used a 2°x2.5° grid size. When the horizontal resolution is changed, the tuning parameter F should be adjusted. Since the mass flux is not changed, a reduction of moisture flux implies a reduction of the mixing ratio at the interface. According to the mean West Indies sounding (Jordan 1958), the water mixing ratio drops by 26% in the first 1 km in the vertical direction and by another 35% in the second 1 km. A value of 0.33 for F give a reduction factor, R, of 16% if the surface elevation rises by 1 km between neighboring grids in a 2°X2.5° horizontal resolution and if $\cos\varphi$ is 1. Thus, our reduction factor, R, is not outside of the reasonable range. Also, this modification has no effect over ocean grids except those bordering steep mountains.

Strictly speaking, according to Fig 4, when the wind is in the downslope direction (i.e., when cos φ is negative) the moisture flux should be modified as well. However, such a modification should be done carefully to avoid generating negative moisture in the upslope grid box. A test has been made in this direction, but it generated few changes; since the upstream-q-based scheme used in the GEOS-5 GCM gives a moisture amount at the interface comparable to that of the upslope grid box (Fig. 3). Consequently, in our final implementation no modification to the interface moisture flux is done when the flux is downslope. For the GCMs that use interpolation schemes, in computing the interface q, that give roughly equal weights to the q's on both sides of the interface it is advisable to incorporate such a modification.

CICK in the horizontal direction (when the sigma coordinate is used) in the mountainous regions is best dealt with by modifying the horizontal moisture flux according to the Arakawa and Lamb's (1977) analysis. However, again due to our unfamiliarity with the advection part of the code, we rely on the aforementioned reduction in horizontal moisture flux and simply use an F (F=0.5) that is somewhat greater than the F that can be justified by the above analysis (F=0.333), which applies if CICK is not present. Thus, F is used as a tuning parameter and is varied between 0 and 0.5 among various experiments.

Adding any type of additional friction in the boundary layer over mountain slopes does not provide any relief for the EPSM problem. The reason is that adding more friction to the boundary layer over mountain slopes only reduces the upslope wind speed and, therefore, surface heat flux momentarily and then this is immediately followed by a rise in ground temperature and restoration of surface heat flux. The reduced upslope wind speed, by lessening its cooling effect, allows the temperature in the boundary layer to rise; which, by generating higher differential heating in the horizontal direction, in turn, restores the speed of the upslope winds. The net result of increasing friction in the boundary layer over

the mountainous regions is a little delay in the development of the upslope winds during the day and a little higher temperature in the boundary layer during the day. But as far as EPSM is concerned, adding more friction in the boundary layer has very little impact, since the speed of the upslope wind is little changed. We have added the blocked flow drag, a form of boundary layer friction, to the GEOS-5 GCM following the ECMWF formulation (IFS note Chapter 4; see the Appendix for a correction of the IFS notes.) Tests showed little impact on EPSM, as expected.

4. Test results

The SHVC parameterization as described in the preceding section has been tested using the GEOS-5 GCM. A control integration (E001, see Table 1) without and a test integration (E002) with the SHVC parameterization were started from the same set of initial conditions on May 28, 1982 and run till March 1, 1983. This is a period in which EPSM is quite strong. The horizontal grid size we used was 2° (lat.) x2.5° (lon.) and F was set to 0. The resulting DJF precipitation is shown in Fig. 8.a for the two integrations. The test results show that our SHVC parameterization scheme has contributed greatly to the resolution of the EPSM problem in the GEOS-5 GCM. The globally averaged precipitation is hardly changed, but precipitation over the Andes has been improved. The precipitation peak at 22S and 65W over the Andes shifts and extends southeastward in other experiments with similar settings. This suggests that a mechanism different from that of EPSM is at play. Over New Guinea the model now sports a small deficit in precipitation. This is attributed to the difficulty in simulating the ITCZ intensity and location and it is not an indication of a problem with our approach.

Over the oceans there is generally a deterioration of the DJF ITCZ simulation. For example, the DJF ITCZ simulation in the northern Indian Ocean has become somewhat stronger than before. This can also be attributed to the difficulty in the ITCZ simulation. This is an example of a relatively good simulation of a feature in the model being the result of the partial cancellation of two model systematic errors, one helps and the other hurts the simulation of this particular feature. When the one that helps the simulation is removed or reduced (in an effort to solve a separate problem), the simulation becomes worse. Exactly why our treatment for EPSM leads to the deterioration of the DJF ITCZ simulation remains to be determined. There was considerable amount of tuning effort that went into the model, prior to our treatment of EPSM, to reduce the ITCZ systematic errors (Bacmeister et al. 2006). It is not surprising that after our treatment of the EPSM problem is implemented this tuning must be redone to maintain the performance level of the ITCZ simulation. However, re-tuning may not be such a desirable approach, since why the tuning helped in the first place has not been understood. Thus, further theoretical study of the ITCZ simulation is essential. Nevertheless, the deterioration of the ITCZ simulation in the Indian Ocean and in the western Pacific in DJF is compensated by the improvement in the precipitation rate just south of the equator in the Indian Ocean and over Australia and in the oceanic region to the northwest of Australia. More importantly, the standard deviation of the precipitation difference between the simulation results and the GPCP data in DJF, as shown in the bottom panels of Fig. 8a, is improved by more than 10% (Table 2.)

In the JJA season precipitation over the Himalayas exhibits great improvement (Fig. 8.b). Similar improvements are seen in the Ethiopian Highland, New Guinea, Mexico, and the Andes. Moreover, the globally-averaged standard deviation of the JJA precipitation error is reduced by as much as 18%. Both sea level pressure (Fig. 9) and 500 hPa height (Fig.10) error fields show more than a 20% improvement in their standard deviations of the

error fields in the JJA season. These difference fields show the impact of our approach reaching beyond the steep and high mountain regions. This is expected given the extended reach of the vertical circulation associated with the resolvable upslope flow and various types of global tele-connection pattern, scale interaction and instability in the atmospheric general circulation.

Fig. 11 shows the before and after (E001 vs. E002) plots of the January (1983) mean diurnal cycle of precipitation at 22S across South America. Since the total precipitation over the Andes has been reduced, the amplitude of the precipitation diurnal cycle there is reduced as well. However, there is no change in the phase of the diurnal cycle of precipitation over the Andes. Fig 12 shows the same for zonal wind at 50m (U50m) above ground and Fig. 13 shows the vertical cross section of January mean u wind at 21Z, the peak time (about 4~5 pm local time) of Andes U50m before our treatment. These plots show that the winds converging toward the Andes (centered around 67W) from both sides have been reduced and that the corresponding precipitation rate has been reduced as well.

In a separate integration E002 was extended to cover the period of June 1982 to Feb 1991. The resulting DJF and JJA precipitation averaged over the entire period (not shown) reveals that the EPSM problem has been removed in other years as well.

Another test run (E003) the same as E002 but with $\alpha = 0$ showed comparable results. However, there is some deterioration in the standard deviation of the error fields (Table 2).

In a separate experiment (E004) the reduction of interface q is added by setting F to be 0.5 with α remaining at 1. The results are very similar to those of E002 as far as solving the ESPM problem is concerned. This is not surprising given the fact that the SHVC parameterization provides much of the cure and the fact that there is not much room left for the reduction of interface q to show its contribution. By itself the reduction of interface q

with F=0.5 can provide only about 20% of the cure. EPSM is prevented when the boundary layer moisture flux qv on the resolvable scale slopes is sufficiently reduced. Parameterization of SHVC reduces v substantially and then, with reduced v, q is reduced on the slopes due to weaken upslope moisture flux (and the ventilation of moisture by SHVC). Thus, qv is reduced substantially by the SHVC parameterization. Reduction of interface q by itself only reduces q in a limited manner. The feedback of reduced q on v is similarly limited. When both SHVC parameterization and reduction of interface q are employed their effects are not additive. In summary, E002 gives the best overall results (see Table 2).

5. Discussions and summary

In this study, we have explored the possible causes of EPSM, which is a common problem among atmospheric models, and have presented our solutions. The principal cause is, by far, a lack of ventilation of heat upward from the boundary layer by the sub-grid scale vertical circulations (SHVC), which are forced by the subgrid-scale boundary layer upslope winds. SHVC are associated with large subgrid-scale topographic variation, which is found over steep and high mountains. A lesser cause is a poorly-designed horizontal moisture flux (coupled with a terrain-following vertical coordinate), which does not recognize the variation in surface elevation between neighboring grids. The other possible causes examined are a lack of blocked-flow drag, cumulus convection being too easily triggered at high elevations and conditional instability of the computational kind, but they turned out to be inconsequential. We have designed a solution by parameterizing the heat ventilation effect of the SHVC. Also, the horizontal moisture flux is reduced between neighboring grids that vary in surface elevation, and the amount of reduction is proportional to the difference in surface elevation. Our solution is crude but effective.

Further refinement of our solution will be possible when more research is done to illuminate the nature of SHVC, such as high-resolution simulations, and when more observational data are available.

Although the causes we have identified and the test results of our solution appear to be reasonable, our study has not discounted the possibility of other minor contributing factors to the problem at hand besides the ones we have identified. Our solution of incorporating the parameterization of SHVC might have been overdone to correct errors due to other unknown minor causes. Of course, this kind of caution should be taken for most corrections to the problems in GCMs. It is likely that with further improvement in other aspects of the model, such as boundary layer heating and friction and convection parameterization, the amount of heat ventilation described in Section 3 will need to be adjusted.

In Section 2 we brought up the larger surface area under a grid column due to the topographic variation as a possible concern in the EPSM problem. The larger surface area has impact on the magnitude of various surface fluxes. However, we do not expect their roles in the EPSM problem to be of any greater importance than, or of an importance anywhere close to, the heat ventilation effect of SHVC. The reason for this expectation is that the heat ventilation effect has to remove almost all of the heating tendency due to surface heat flux in the boundary layer on mountain slopes in order to avoid EPSM and this large amount of heating reduction cannot be achieved by the fractional change and repartitioning of surface fluxes associated with taking into account the larger surface area due to topographical variation within a grid. Nevertheless, the larger surface area associated with topographical variation is a topic that deserves attention in future studies.

It should be obvious by now that as the model horizontal resolution is increased, the dosage needed for the SHVC parameterization, like that for the gravity wave

parameterization, becomes less. Thus, when the horizontal resolution is increased, all the tuning parameters R_{SV}, α, and Zbot should be adjusted.

As mentioned in the introduction, multi-scale modeling framework (MMF) models, like their host GCMs, also exhibit EPSM. The reason is now clear from our study: the cloud-resolving models used within the MMF models assume that the bottom surface is level and flat. In the future when the bottom surface topographic variation is allowed in the cloud-resolving models, SHVC will be simulated and the MMF models will avoid the EPSM problem. It is advisable to put the correction for the interface moisture in the host GCM. Of course, it would be highly desirable for an MMF model to have the same horizontal resolution for the land-surface model as that for the cloud-resolving model.

The solutions that we have devised have been shown to be able to avoid the EPSM problem. However, like any other parameterizations, our SHVC parameterization has considerable room for improvement. One obvious area is our treatment and non-treatment for SHVC moisture and momentum fluxes, respectively. One problem with our treatment of the SHVC moisture transport is that part of the uplifted moisture in SHVC may condense and release latent heat and this is not included in our treatment. It is unlikely that the cumulus parameterization scheme and the large-scale moist processes used in the model can handle this correctly. Even with these blemishes we have obtained very encouraging results. This indicates that the SHVC moisture and momentum fluxes are not crucial as far as solving the EPSM problem is concerned. Also, there is no parameterization scheme that is perfected on the first attempt. Thus, given the overall improvement our treatment has yielded, things to be improved should be deemed as refinements rather than critical needs. If the history of cumulus convection and planetary boundary layer parameterizations is any guide, we expect that the improvement in the SHVC parameterization will take a long time. Whether cumulus parameterization and SHVC parameterization should be and/or can be combined

as a single convection parameterization is worth contemplating. As mentioned earlier, observational knowledge about SHVC needs to be greatly expanded. Also, more modeling effort with high-resolution regional models will be very useful.

In a nutshell, while the mechanical effects of sub-grid scale topographic variation have long been recognized and incorporated in the atmospheric models as envelope topography and the gravity-wave and blocked-flow drag parameterizations, this study has shown that the corresponding thermal effects should also be recognized and incorporated as the SHVC parameterization in order to prevent EPSM.

Acknowledgments. Technical help from Larry Takacs, Max Suarez, and Andrea Molod, all of GMAO/GSFC/NASA, in using the GEOS-5 GCM is gratefully acknowledged. This research was supported by NASA's Modeling, Analysis and Prediction program under WBS 802678.02.17.01.25. Computing resources supporting this work were provided by the NASA High-End Computing (HEC) Program through the NASA Center for Computational Sciences (NCCS) at Goddard Space Flight Center.

APPENDIX

Correction of the angle between the principal axis of the topography and the x-axis in the ECMWF/IFS documentation

Eq. 4.22 of the ECMWF/IFS documentation, Part IV (2006) gives the angle between the principal axis of the topography and the x-axis as $\theta = 0.5 \arctan(M/L)$ (with all notations defined in the IFS documentation). This formula, also appearing in Baines (1995), gives a value between $-\pi/4$ and $\pi/4$; whereas in fact θ varies between $-\pi/2$ and $\pi/2$. The corrected equation is:

$\theta = 0.5 \arctan(M/L)$, if $L>0$,

$\theta = 0.5 \arctan(M/L) + \pi/2$, if $L<0$ and $M>0$, and

$\theta = 0.5 \arctan(M/L) - \pi/2$, if $L<0$ and $M<0$.

Moreover, the $\overline{h}$ on the same page of the document should be interpreted as a function of x and y rather than a constant in the model grid box. It can be approximated by a plane least-squares-fitted to h within the grid box.

References

Arakawa, A. and V. R. Lamb, 1977: Computational design of the basic dynamical processes of the UCLA general circulation model. Book chapter, *General circulation models of the atmosphere*." (J. Chang, Ed.) *Methods in Computational Phys.* Vol. **17**, 173-265. Academic Press.

Bacmeister, J. T., M. J. Suarez, and F. R. Robertson, 2006: Rain re-evaporation, boundary-layer/convection interactions, and Pacific precipitation patterns in an AGCM, *J. Atmos. Sci.*. **63**, 3383-3403.

Baines, P. G., 1995: *Topographic effects in stratified flows.* Cambridge University Press. 482 pp.

Bosilovich, M. G., F. R. Robertson and J. Chen, 2011: Global energy and water budgets in MERRA. *J. Climate* (submitted).

Chou, M.-D., M. J. Suarez, X. Z. Liang, and M. M.-H. Yan, 2001: A Thermal Infrared Radiation Parameterization for Atmospheric Studies. NASA *Technical Report Series on Global Modeling and Data Assimilation 104606*, **v19**, 56pp.

Chou, M. D. and M. J. Suarez, 1999: A solar radiation parameterization for atmospheric studies. *NASA Technical Memo*, 104606, **11**, 40 pp.

Delworth, T. L., 2006: GFDL's CM2 global coupled climate models. Part I: Formulation and simulation characteristics. *J. Clim.*, **19**, 643-674.

ECMWF/IFS documentation, 2006: Integrated Forecast System Documentation – Cy31r1, Operational implementation 12 September 2006. Available at http://www.ecmwf.int/research/ifs/ .

Garcia, R.R. and B.A. Boville, 1994: Downward control of the mean meridional circulation and temperature distribution of the polar winter stratosphere. *J. Atmos. Sci*.,

51, 2238–2245.

Jordan, C. L., 1958: Mean sounding for the west Indies area. *J. Meteor*., **15**, 91-97.

Koster, R. D., M. J. Suarez, A. Ducharne, M. Stieglitz, and P. Kumar, 2000: A catchment-based approach to modeling land surface processes in a GCM, Part 1, Model Structure. *J. Geophys. Res.*, **105**, 24809-24822.

Lin, S.-J., 2004: A ''vertically Lagrangian'' finite-volume dynamical core for global models. *Mon. Wea. Rev*. **132**, 2293-2307.

Lock, A. P., A. R. Brown, M. R. Bush, G. M. Martin, and R. N. B. Smith, 2000: A new boundary layer mixing scheme. Part I: Scheme description and single-column model tests. *Mon. Wea. R*ev., **128***,* 1387-1399.

Lord, S. J., W. C. Chao and A. Arakawa, 1982: Interaction of a cumulus cloud ensemble with the large-scale environment. Part IV: The discrete model. *J. Atmos. Sci.*, **39**, 104-113.

Louis, J. F., 1979: A parametric model of vertical eddy fluxes in the atmosphere*. Boundary Layer Meteor.*, **17***,* 187-202.

Ma, H.-Y., C. R. Mechoso, Y. Xue, H. Xiao, C.-M. Wu, J.-L. Li, and F. De Sales, 2011: Impact of land surface processes on the South American warm season climate. *Climate Dyn*., doi:10.1007/s00382-010-0813-3, **37**,187–203.

McFarlane, N. A., 1987: The effect of orographically excited gravity wave drag on the general circulation of the lower stratosphere and troposphere. *J. Atmos. Sci.*, **44**, 1775-1800.

Moorthi, S., and M. J. Suarez, 1992: Relaxed Arakawa-Schubert: A parameterization of moist convection for general circulation models. *Mon. Wea. Rev.,* **120***,* 978-1002.

Oouchi, K., A. T. Noda, M. Satoh, B. Wang, S.-P. Xie, H. G. Takahashi, and T. Yasunari, 2009: Asian summer monsoon simulated by a global cloud-system resolving model: Diurnal to intra-seasonal variability. *Geophys. Res. Lett.*, **36**, L11815.

Rampanelli, G., D. Zardi, and R. Rotunno, 2004: Mechanisms of upslope winds. *J. Atmos. Sci.,* **61**, 3097-3111.

Da Rocha R. P., C. A. Morales, S. V. Cuadra, and T. Ambrizzi, 2009: Precipitation diurnal cycle and summer climatology assessment over South America: An evaluation of regional climate model version 3 simulations. *JGR*, **114**, D10108, doi:10.1029/2008JD010212

Tao, et al., 2009: A multi-scale modeling system: Developments, applications, and critical issues. *Bull. AMS*, 519-534.

de Wekker, S. F. J., S. Zhong, J. D. Fast and C. D. Whiteman, 1998: A numerical study of the thermally driven plain-to-basin wind over idealized basin topographies *J. Appl. Meteor*., **37**, 606-622.

Table 1. Experiments

E001	Control experiment without any of our changes
E002	Experiment with the ventilation effect of subgrid scale vertical circulation, with removal of moisture from the PBL (α=1), but without reduction of horizontal moisture flux when the flow is upslope (F=0.)
E003	Same as E002 but without removal of moisture from the PBL and its deposit at higher levels (α=0)
E004	Same as E002, but with reduction of horizontal moisture flux when the flow is upslope (F=0.5).

Table 2. Standard Deviation of Error Fields

(Error being the difference between simulation results and the observational data, as shown in the bottom panels of Figs. 8-10)

Experiment	E001	E002	E003	E004
DJF				
Precip (mm/day)	2.156	1.960	1.903	1.957
500mb Height (m)	44.964	49.878	50.839	50.157
500mb Eddy Height (m)	32.191	30.632	33.712	31.978
500mb T (K)	1.309	1.377	1.648	1.635
SLP(hPa)	4.436	4.628	5.177	5.011
JJA				
Precip (mm/day)	2.291	1.877	2.066	1.931
500mb Height(m)	37.192	26.746	32.904	27.876
500mb Eddy Height(m)	27.559	20.936	27.695	22.839
500mb T(K)	1.350	1.174	1.162	1.140
SLP(hPa)	4.325	3.381	3.578	3.573

Figure Captions

Fig. 1. Schematic diagram showing the vertical circulation forced by the boundary layer heating on the resolvable scale.

Fig. 2. Schematic diagram showing the vertical circulation forced by boundary layer heating on the subgrid scale.

Fig. 3. Schematic diagram showing two neighboring grid boxes at the bottom layer in a terrain following coordinate.

Fig 4. Exponential vertical profile of water mixing ratio q between two horizontally neighboring grids in a terrain-following vertical coordinate, which have grid center heights at Z1 and Z2. The difference between q at the interface, if interpolated linearly from q1 and q2, and the true value is shown by the line with arrows at both ends. This difference becomes much larger when q at the interface is extrapolated from the upstream side and when the wind is blowing upslope.

Fig. 5. Reduction factor R_{SV} applied to the turbulence heating in the boundary layer as a function of the standard deviation of the topography.

Fig. 6. Variation of topography along 22S and along 68W over South America using USGS GTOPO30 data with 1km resolution.

Fig. 7. Schematic diagram showing the return flow, denoted by the horizontal arrow, responding to heat deposition in the shaded area.

Fig. 8a. Average precipitation (mm/d) in E001 and E002 for one DJF season. The top panels are the model result, the middle panels are GPCP observation, and the bottom panels are the differences (top-middle). The vertical color

bar is for the upper and middle panels. The horizontal color bar is for the bottom panel.

Fig. 8b. Same as Fig.8a but for one JJA season.

Fig. 9. Average sea level pressure difference (model results minus ERA40 observations, in hPa) in E001 and E002 for one DJF season (upper panels) and for one JJA season (lower panels).

Fig. 10. Average 500 hPa height difference (model results minus ERA40 observations, in meters) in E001 and E002 for one DJF season (upper panels) and for one JJA season (lower panels).

Fig. 11. 1983 January mean diurnal variation of precipitation (mm/day) at 22S across South America (E001 v. E002). The vertical axis is UTC hour.

Fig. 12. Same as Fig. 12 but for zonal wind (m/s) at 50m above ground (E001 v. E002). The vertical axis is UTC hour.

Fig. 13. Vertical cross section at 21Z in the January mean diurnal cycle of zonal wind (m/s) (E001 v. E002).

Rendered Figure.Fig.1
Click here to download Rendered Figure: Fig.1.doc

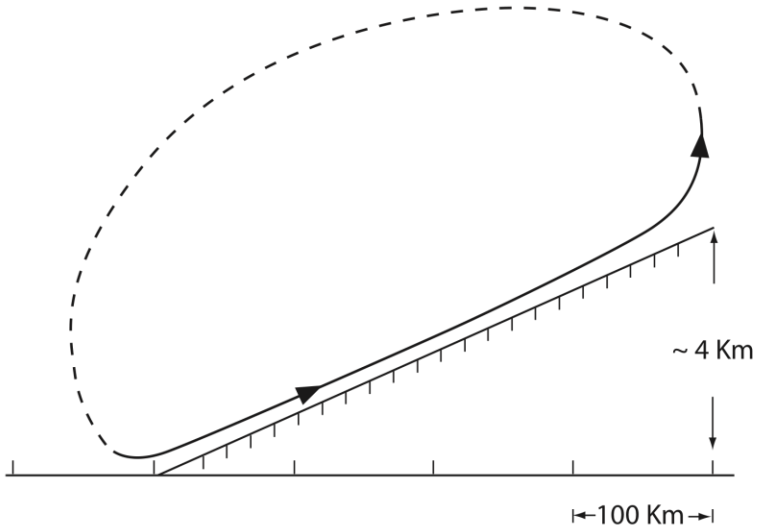

Fig.1 Schematic diagram showing the vertical circulation forced by the boundary layer heating on the resolvable scale.

Rendered Figure.Fig.2
Click here to download Rendered Figure: Fig.2.doc

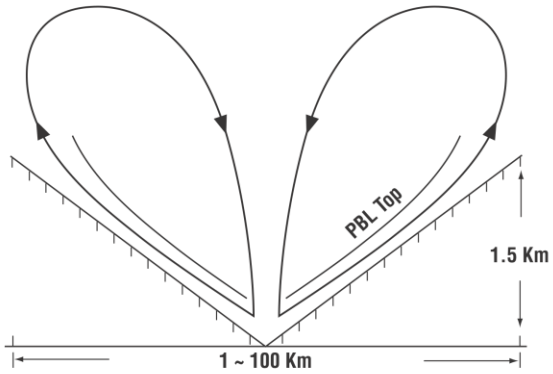

Fig 2. Schematic diagram showing the vertical circulation forced by boundary layer heating on the subgrid scale.

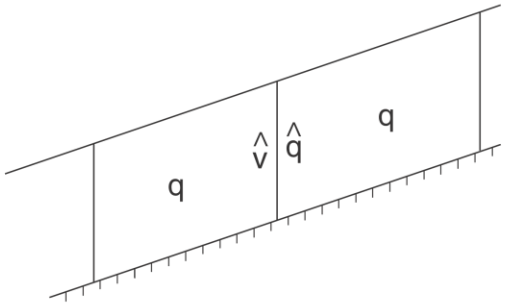

Fig. 3. Schematic diagram showing two neighboring grid boxes at the bottom layer in a terrain following coordinate.

Rendered Figure.Fig.4
Click here to download Rendered Figure: Fig.4.doc

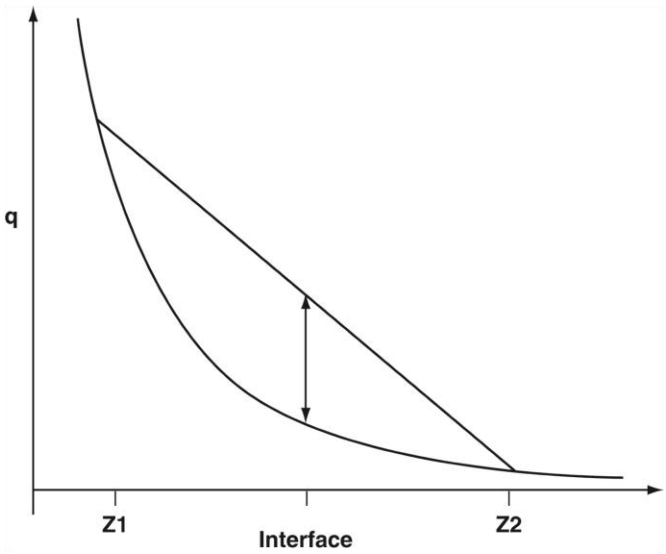

Fig. 4. Exponential vertical profile of water mixing ratio q between two horizontally neighboring grids in a terrain-following vertical coordinate, which have grid center heights at Z1 and Z2. The difference between q at the interface, if interpolated linearly from q1 and q2, and the true value is shown by the line with arrows at both ends. This difference becomes much larger when q at the interface is extrapolated from the upstream side and when the wind is blowing upslope.

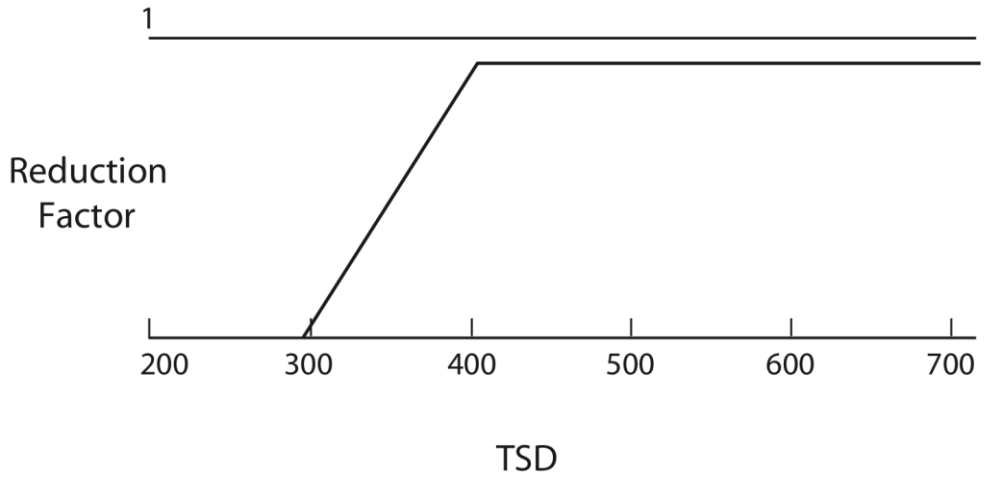

Fig. 5. The reduction factor R_{SV} as a function of standard deviation of topography (in m).

Rendered Figure.Fig.6a
Click here to download Rendered Figure: Fig.6a.doc

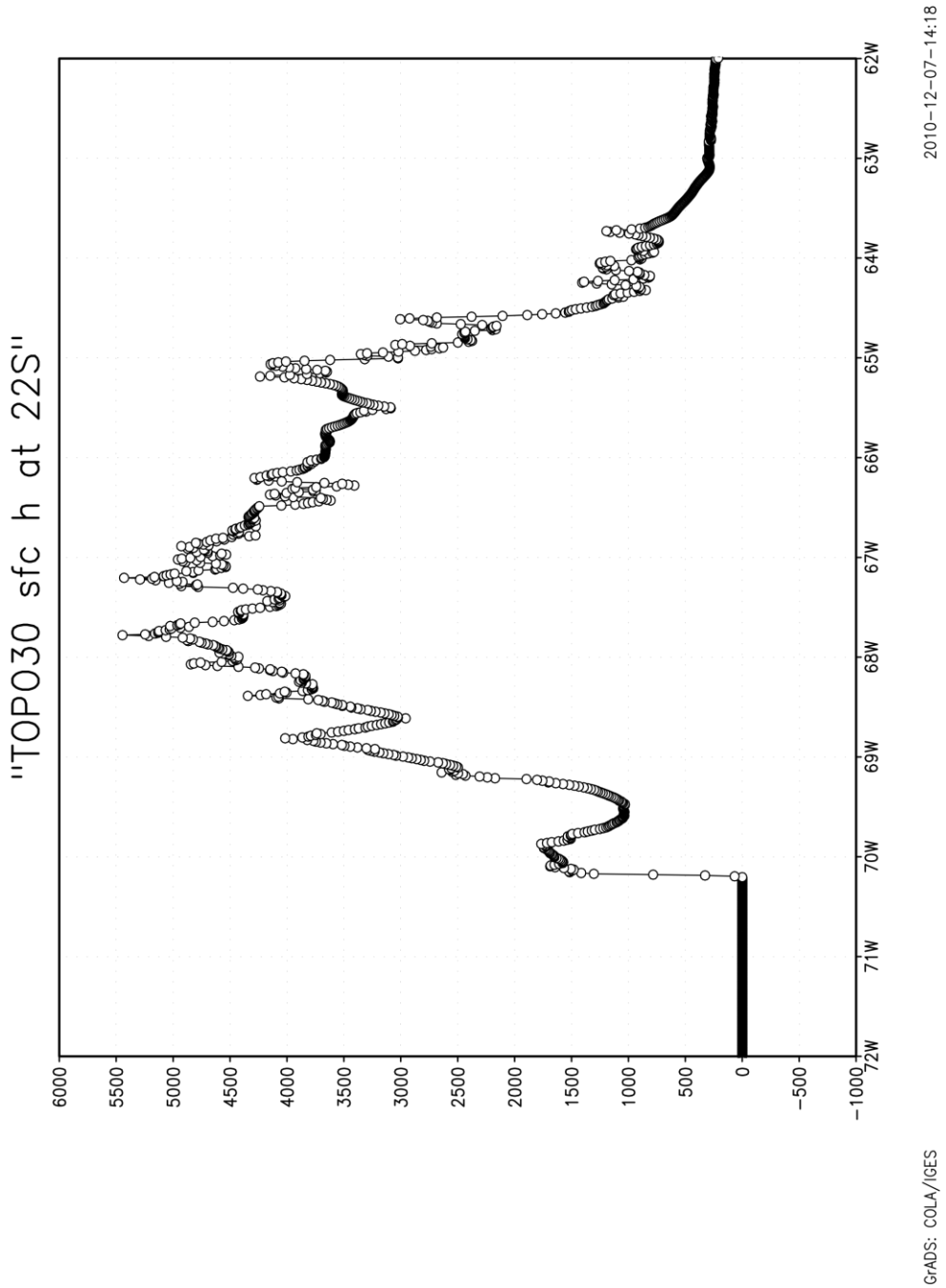

Fig. 6a. Variation of topography along 22S over South America using USGS GTOPO30 data with 1km resolution.

Rendered Figure.Fig.6b
Click here to download Rendered Figure: Fig.6b.doc

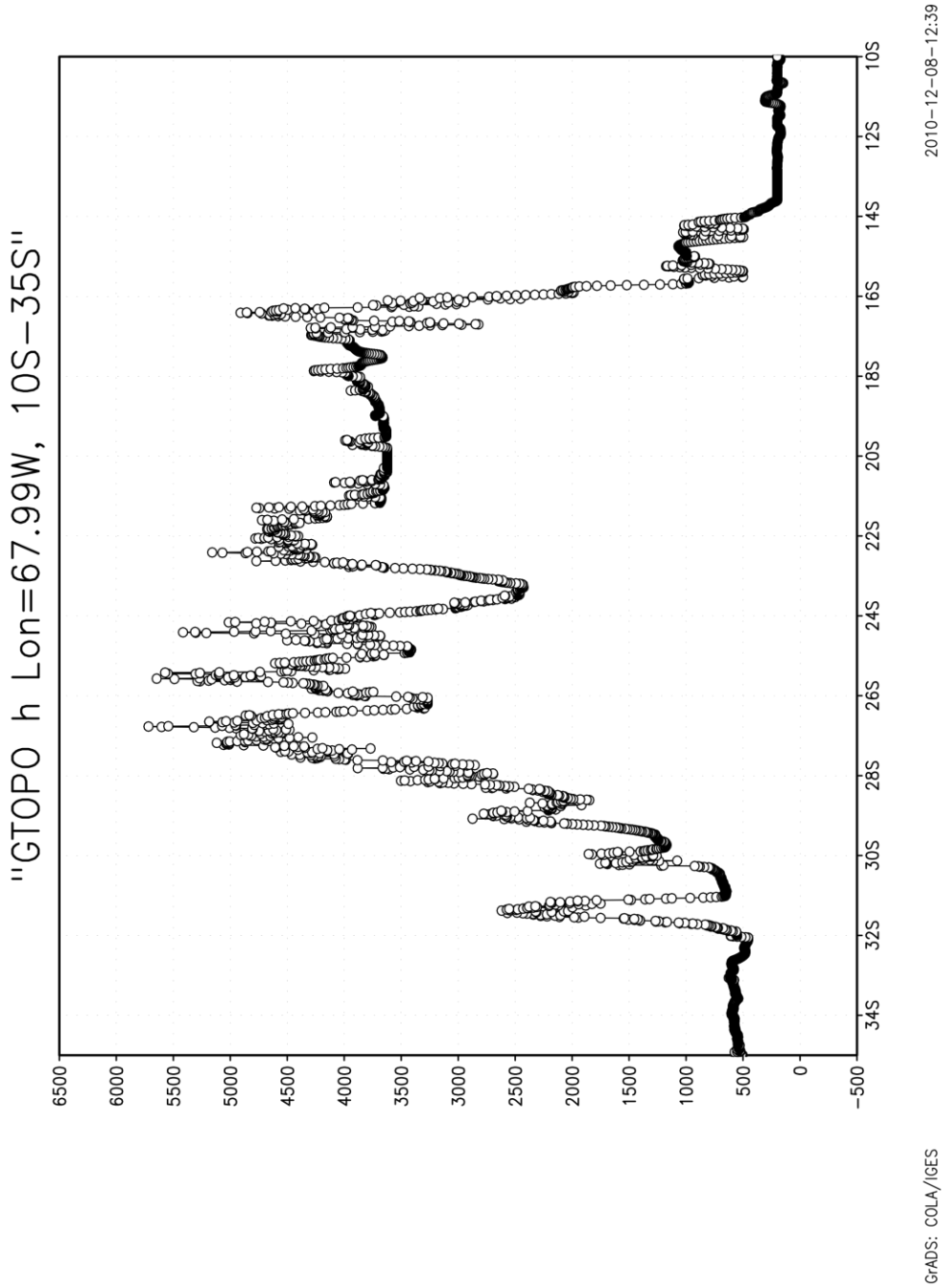

Fig. 6b. Variation of topography along 68W over South America using USGS GTOPO30 data with 1km resolution.

Rendered Figure.Fig.7
Click here to download Rendered Figure: Fig.7.doc

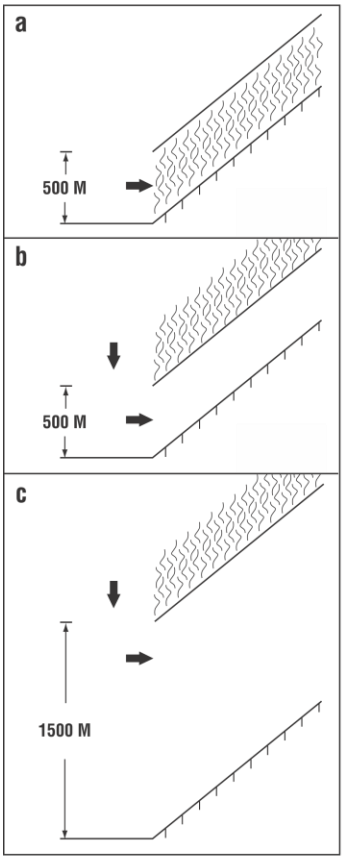

Fig. 7. The return flow, denoted by the horizontal arrow, responding to deposited heating in the shaded area.

Rendered Figure.Fig.8
Click here to download Rendered Figure: Fig.8.doc

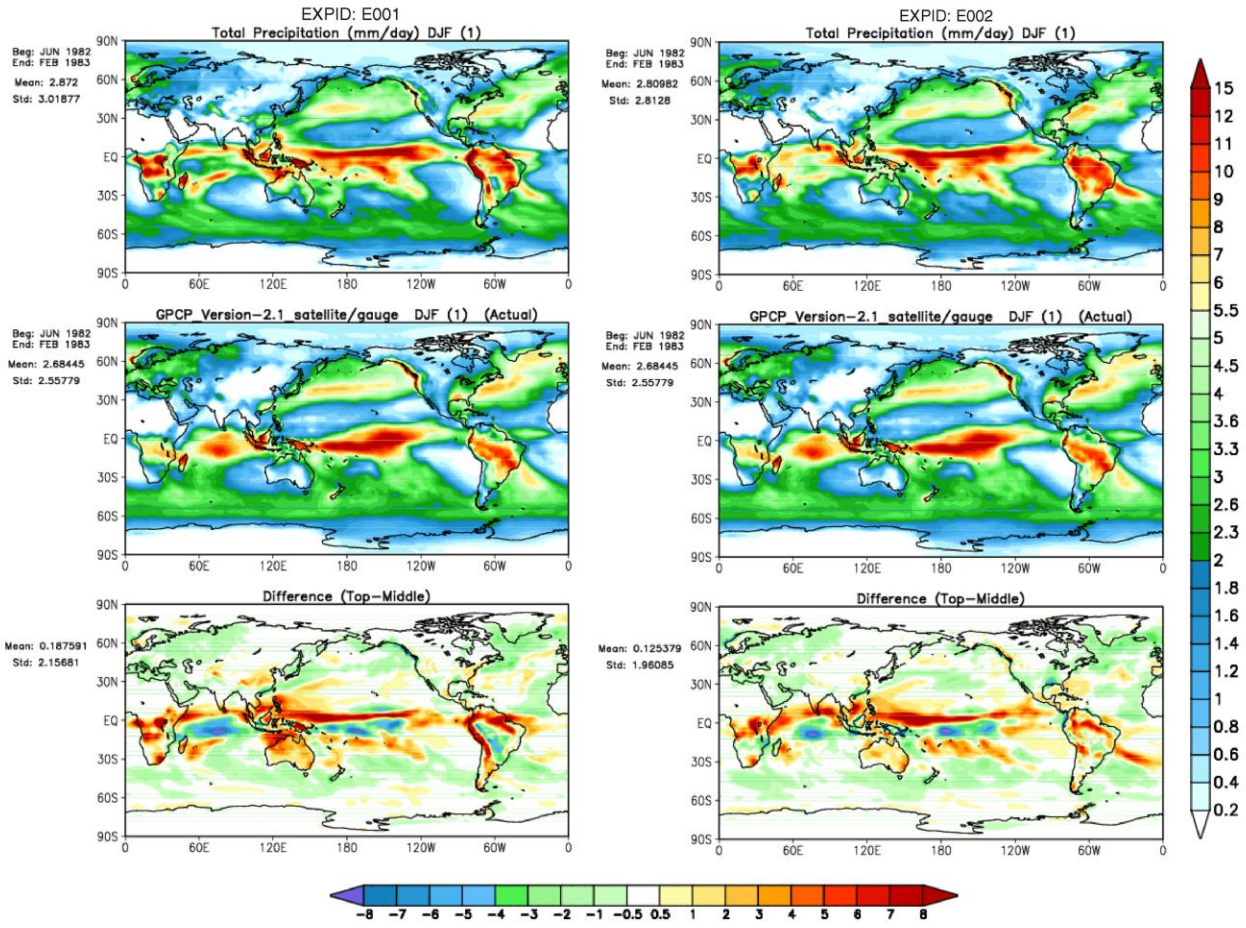

Fig. 8a. Average precipitation (mm/d) in E001 and E002 for one DJF season. The top panels are the model result, the middle panels are GPCP observation, and the bottom panels are the differences (top-middle). The vertical color bar is for the upper and middle panels. The horizontal color bar is for the bottom panel.

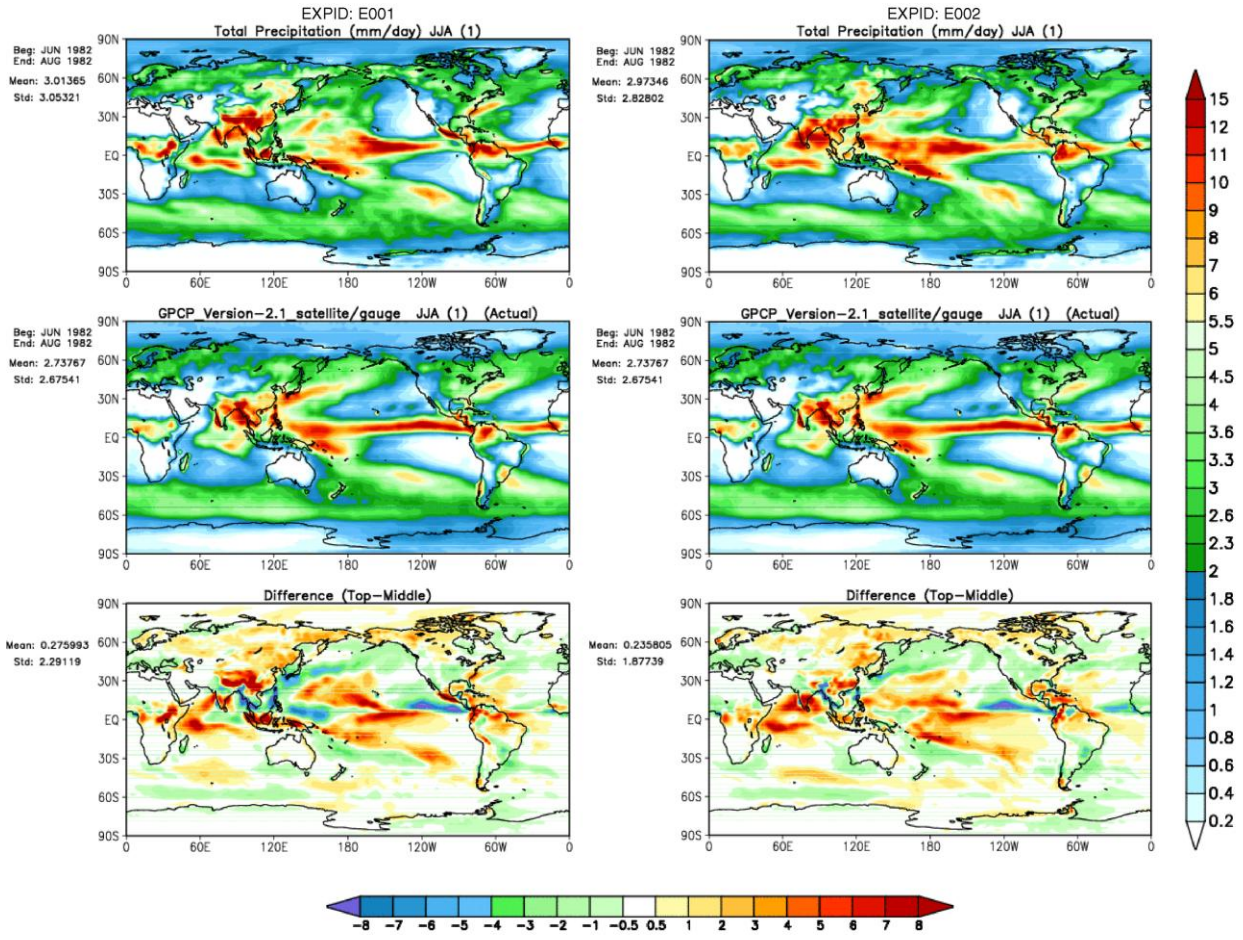

Fig. 8b. Same as Fig.8a but for one JJA season.

Rendered Figure.Fig.9
Click here to download Rendered Figure: Fig.9.doc

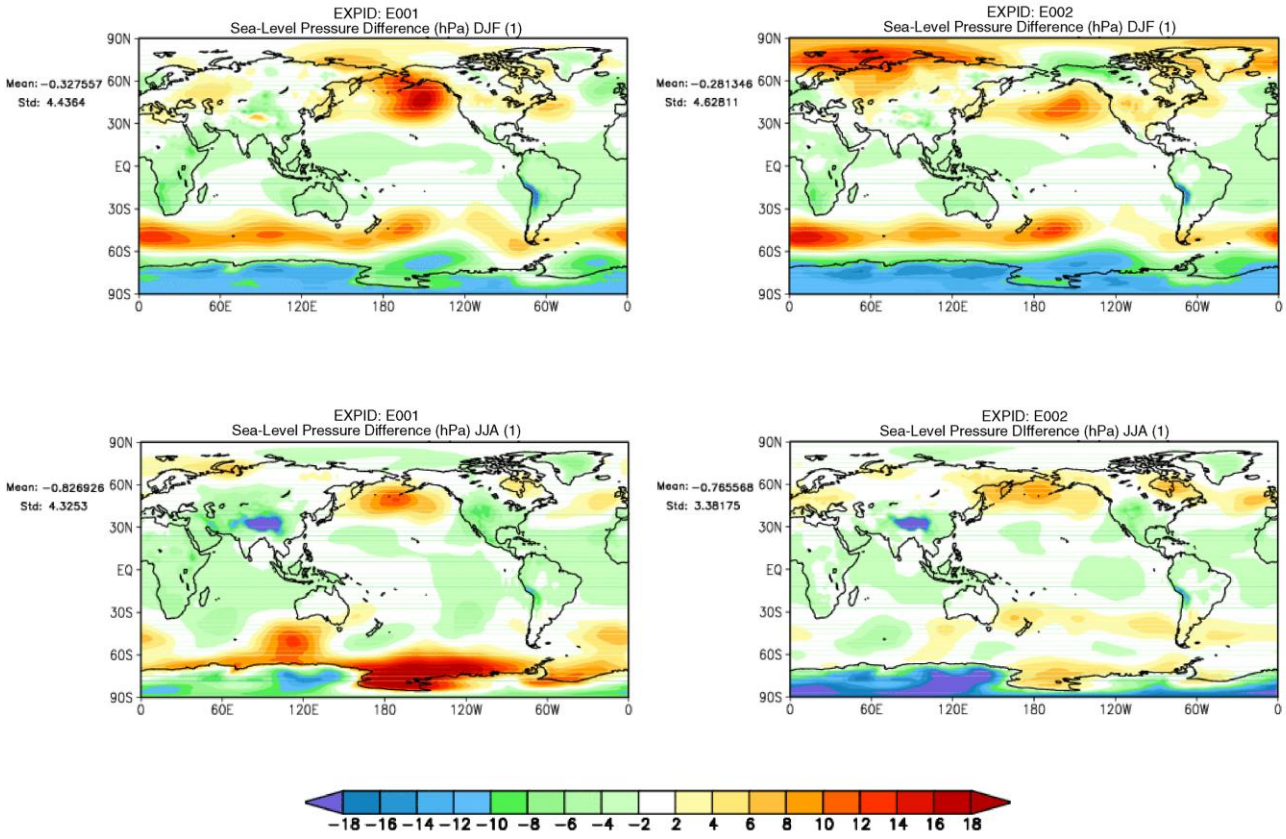

Fig. 9. Average sea level pressure difference (model results minus ERA40 observations, in hPa) in E001 and E002 for one DJF season (upper panels) and for one JJA season (lower panels).

Rendered Figure.Fig.10
Click here to download Rendered Figure: Fig.10.doc

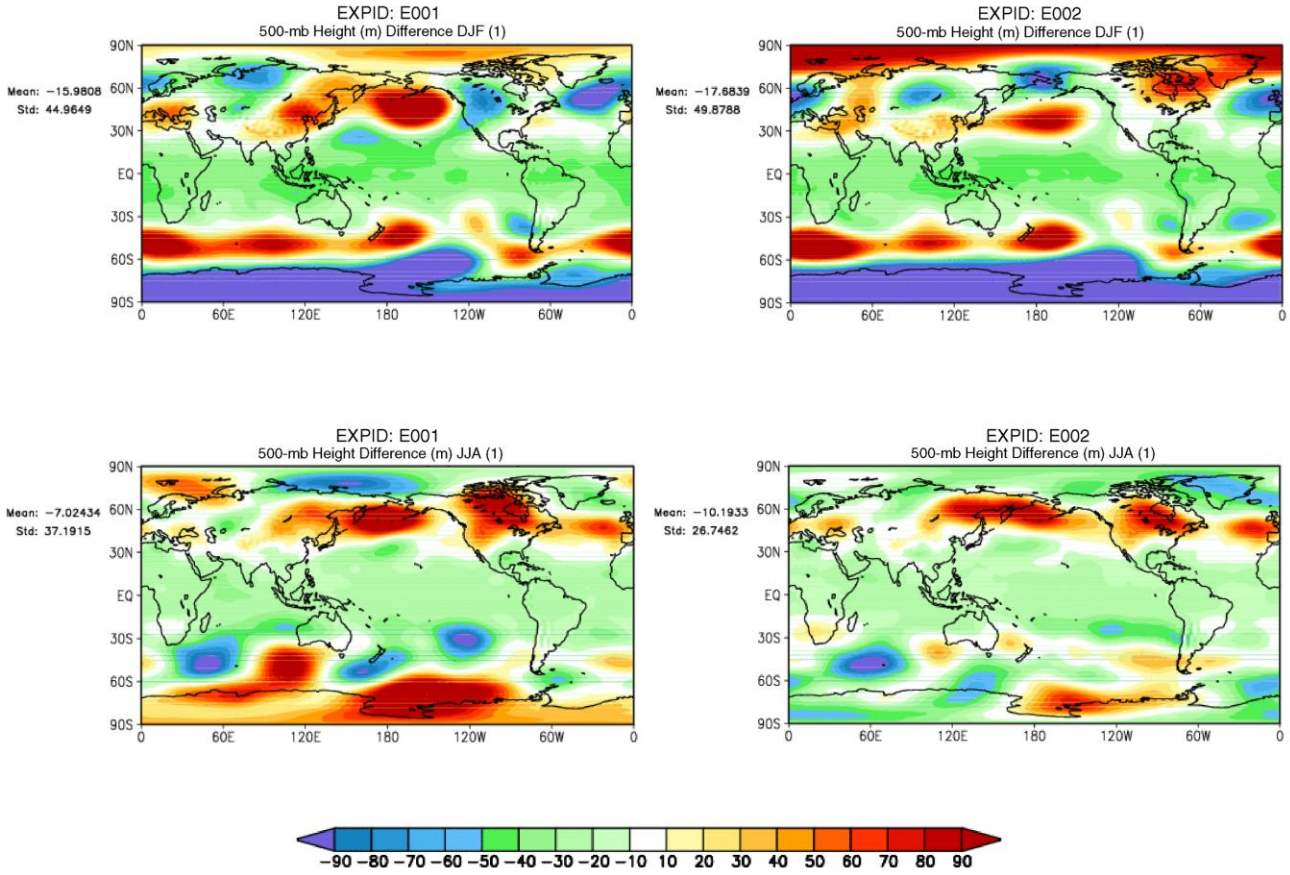

Fig. 10. Average 500 hPa height difference (model results minus ERA40 observations, in meters) in E001 and E002 for one DJF season (upper panels) and for one JJA season (lower panels).

Rendered Figure.Fig.11
Click here to download Rendered Figure: Fig.11.doc

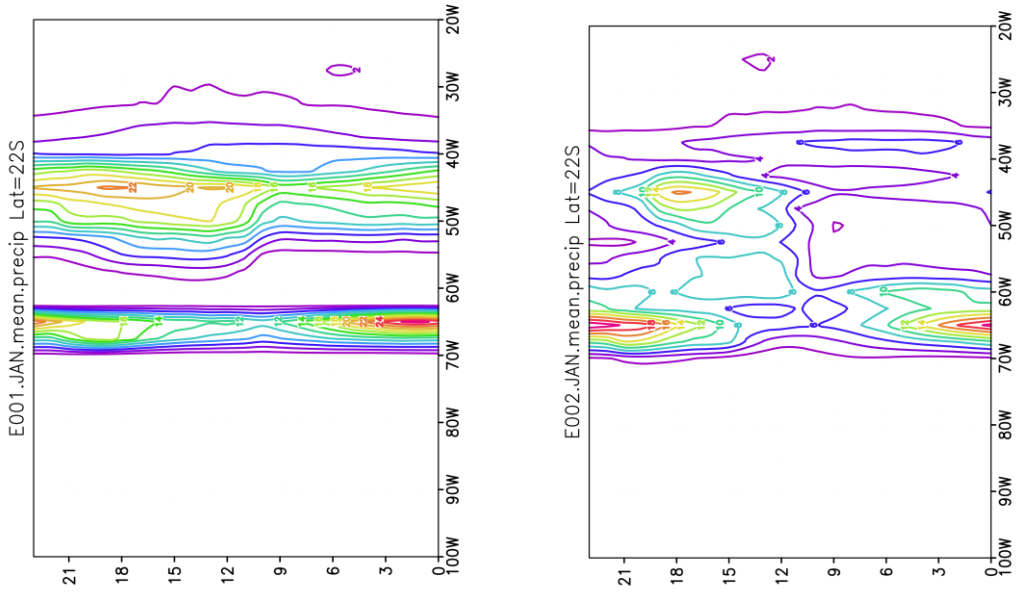

Fig. 11. 1983 January mean diurnal variation of precipitation (mm/day) at 22S across South America (E001 on the left v. E002 on the right). The vertical axis is UTC hour.

Rendered Figure.Fig.12
Click here to download Rendered Figure: Fig.12.doc

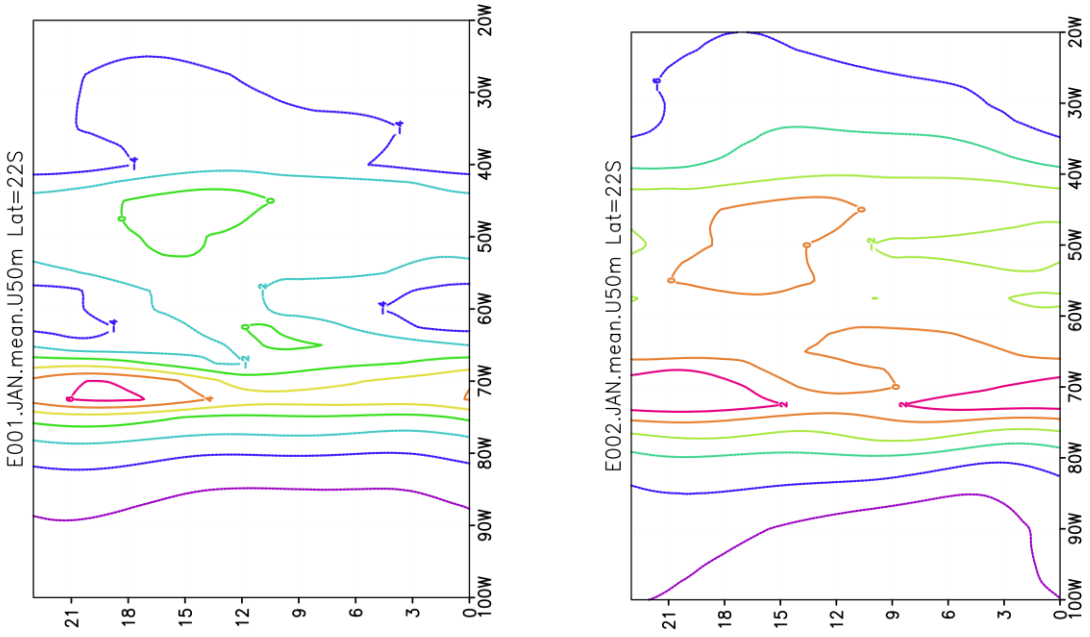

Fig 12. Same as Fig. 12 but for zonal wind (m/s) at 50m above ground (E001 at the top v. E002 at the bottom). The vertical axis is UTC hour.

Rendered Figure.Fig.13
Click here to download Rendered Figure: Fig.13.doc

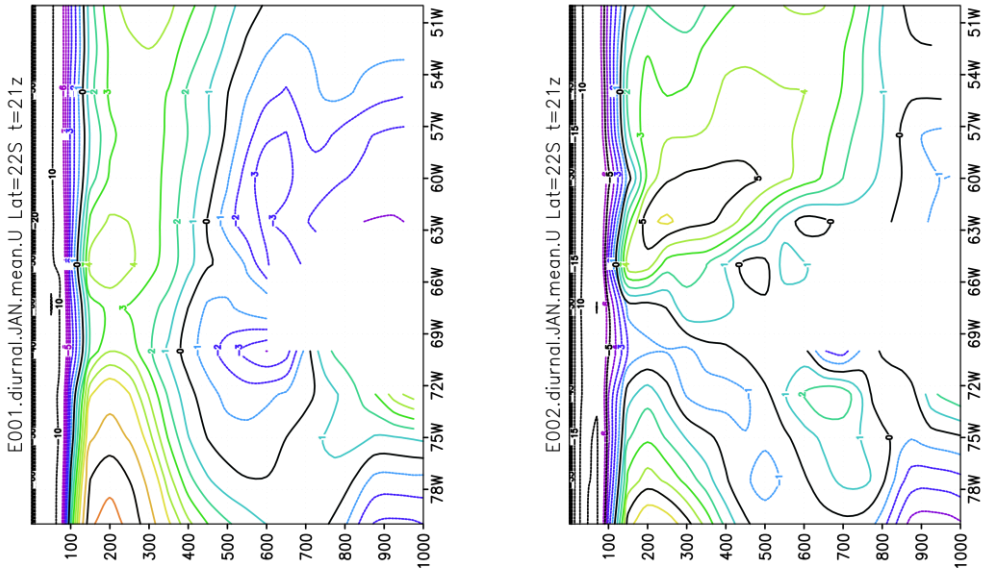

Fig. 13. Vertical cross section at 21Z in the January mean diurnal cycle of zonal wind (m/s) (E001 at the top v. E002 at the bottom). The vertical axis is pressure in hPa.